


Doubly Modulated Optical Lattice Clock: Interference and Topology

Xiao-Tong Lu (卢晓同),^{1,2,‡} Tao Wang (汪涛),^{3,4,‡} Ting Li,^{1,2} Chi-Hua Zhou,^{1,2} Mo-Juan Yin,^{1,2}
Ye-Bing Wang,^{1,2} Xue-Feng Zhang (张学锋) ^{3,4,*} and Hong Chang (常宏)^{1,2,†}

¹Key Laboratory of Time and Frequency Primary Standards, National Time Service Center,
Chinese Academy of Sciences, Xi'an 710600, China

²School of Astronomy and Space Science, University of Chinese Academy of Sciences, Beijing 100049, China

³Department of Physics, and Center of Quantum Materials and Devices, Chongqing University, Chongqing 401331, China

⁴Chongqing Key Laboratory for Strongly Coupled Physics, Chongqing, 401331, China

 (Received 27 September 2020; revised 23 February 2021; accepted 9 June 2021; published 14 July 2021)

The quantum system under periodical modulation is the simplest path to understand the quantum nonequilibrium system because it can be well described by the effective static Floquet Hamiltonian. Under the stroboscopic measurement, the initial phase is usually irrelevant. However, if two uncorrelated parameters are modulated, their relative phase cannot be gauged out so that the physics can be dramatically changed. Here, we simultaneously modulate the frequency of the lattice laser and the Rabi frequency in an optical lattice clock (OLC) system. Thanks to the ultrahigh precision and ultrastability of the OLC, the relative phase could be fine-tuned. As a smoking gun, we observed the interference between two Floquet channels. Finally, by experimentally detecting the eigenenergies, we demonstrate the relation between the effective Floquet Hamiltonian and the one-dimensional topological insulator with a high winding number. Our experiment not only provides a direction for detecting the phase effect but also paves a way in simulating the quantum topological phase in the OLC platform.

DOI: [10.1103/PhysRevLett.127.033601](https://doi.org/10.1103/PhysRevLett.127.033601)

Introduction.—Floquet engineering is a powerful tool for quantum simulating the exotic Hamiltonian via time-periodic driving [1–7]. Extending modulation from one parameter to two is a tantalizing nontrivial task in both physics and technique aspects. The relative phase will strongly change physics due to the time-reversal symmetry breaking [4,8,9], and the typical phenomenon is the observation of interference. Various theoretical proposals of double modulation are discussed, such as realizing the unconventional Hubbard model [10,11], studying quantum scar [12], and controlling particles' migration [13]. However, the experimental realization is extremely hard in the quantum many-body systems because it technically requires both parameters to be independently fine-tuned to make the relative phase ultrastable, and the resulting phenomena can be clearly observed.

As one of the most accurate platforms, the optical lattice clock system becomes an ideal candidate [14–16]. The OLC is composed of an optical local oscillator stabilized by an appropriately chosen two energy levels of transition of thousands of atoms trapped in a lattice potential [17–20]. The lattice laser at “magic wavelength” guarantees both energy levels feel the same lattice potential and the linewidth of the spectrum can be suppressed to several hertz. Meanwhile, the long lifetime of the excited state keeps the system unaffected by spontaneous emission during measurement. Thus, it is not only taken as the candidate of the next standard of time but also as a perfect

platform for measurements of fundamental constants in physics [21–23].

In this Letter, we successfully design and implement an experiment to simultaneously modulate the internal levels of an atom as well as the Rabi frequency in the ⁸⁷Sr OLC system [Fig. 1(a)] [14–16,24]. It can be taken as an effective magnetic field $\vec{h}(t) = \{h_x(t), 0, h_z(t)\}$ coupled to two energy levels in the description of the Pauli matrix $\vec{\sigma}$. The Hamiltonian can be written as

$$\hat{H} = \hbar \vec{h}(t) \cdot \vec{\sigma}. \quad (1)$$

The longitude field $h_z(t)$ is equal to $[\delta + A \cos(\omega_s^z t + \psi)]/2$, where $\delta = \Delta - \omega_p$ is the detuning frequency between the atom internal energy gap Δ and the clock laser photons ω_p ; and the associate modulation is characterized with the longitude driving frequency ω_s^z , amplitude A , and phase ψ . Meanwhile, the transverse field $h_x(t)$ is $\Omega_{\vec{n}} \cos(\omega_s^x t)/2$, where $\Omega_{\vec{n}}$ is the static Rabi frequency of the external harmonic oscillator state $|\vec{n}\rangle$ without modulations and ω_s^x is the transverse driving frequency. In order to check the phase effect, we set $\omega_s^x = \omega_s^z = \omega_s$. Owing to the high precision spectrum in the OLC platform [25], the Floquet sidebands can be resolved at a driving frequency down to 100 Hz [26] so that we can stabilize and fine-tune the relative phase, which remarkably changes the movement path of $\vec{h}(t)$. Because of longitude modulation, the

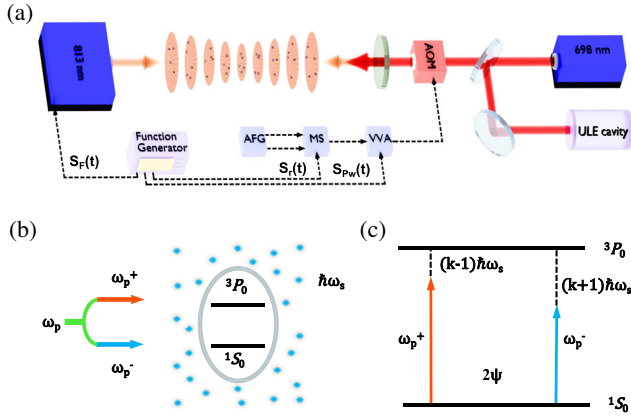


FIG. 1. Schematic picture of experiment setup and interference. (a) Function generator providing three signals: $S_F(t)$, $S_r(t)$, and $S_{PW}(t)$. $S_F(t)$ and $S_{PW}(t)$ used for modulating frequency of 813 nm lattice laser and power of clock laser by voltage variable attenuator (VVA), respectively. Signal $S_r(t)$ can be input into microwave switch (MS) to switch two signals, zero and ϕ , generated by the arbitrary function generator (AFG) so that the phase shift due to transverse amplitude modulation can be compensated. The phase, power, and frequency of the 698 nm clock laser [locked to an ultra-low-expansion (ULE) cavity] are simultaneously changed by imposing the signal from VVA to the acousto-optic modulator (AOM). (b) Under longitude modulation, the two-level atom can be treated as surrounded by Floquet photons with energy $\hbar\omega_s$ in the dressed atom picture. (c) Transverse modulation provides two Floquet channels of ω_p^+ and ω_p^- through which the atoms can hop from 1S_0 to 3P_0 with the assistance of longitude Floquet photons. The relative phase 2ψ between two hopping processes causes interference.

transition between two levels can be assisted by longitude “Floquet photons” with the energy $\hbar\omega_s$. On the other hand, the transverse modulation of the clock laser results in two Floquet channels with “photon frequencies” of $\omega_p^- = \omega_p - \omega_s$ and $\omega_p^+ = \omega_p + \omega_s$, respectively. As shown in Figs. 1(b) and 1(c), when the energy gap Δ is equal to $\omega_p^- + (n_d + 1)\omega_s = \omega_p^+ + (n_d - 1)\omega_s$ (n_d is the order of Floquet sideband), the initial relative phase can induce the interference between Floquet photon assisted tunnelings through two different transverse Floquet channels. Furthermore, the effective Floquet Hamiltonian can be taken as two effective magnetic fields with different winding numbers coupled to atoms. It is directly related to the one-dimensional (1D) topological insulator, and a different Floquet sideband exhibits strong relations with the high order winding number.

Experiment setup.—Approximately 5×10^4 fermionic ^{87}Sr atoms are cooled down to $\approx 3 \mu\text{K}$ and loaded into a quasi-one-dimensional optical lattice aligned with the z axis (experimental details shown in Supplemental Material [26]). As shown in Fig. 1(a), the lattice is created by a counterpropagating laser beam at a magic wavelength of $\lambda_L = 813.42 \text{ nm}$ so that the dipole-forbidden transition

energy levels ($5s^2\ ^1S_0(|g\rangle)$ and ($5s5p\ ^3P_0(|e\rangle)$) feel the same lattice potential. About $N_L \approx 1200$ lattice sites are separated by barriers of height $V_0 \approx 90E_r$ ($E_r = 3.44 \text{ kHz}$, which is the recoil energy), which is strong enough to hinder intersite tunneling. The lifetime of the excited state is about 160 s, whereas each round of the experiment lasts for several hundreds of milliseconds; and so the spontaneous emission could be ignored. Our platform could be well described as an ensemble of noninteracting atoms taking a pseudo-spin half trapped in a harmonic trap [26]. All the atoms are prepared at the ground internal states $|g\rangle$, whereas the distribution at external states $|\vec{n}\rangle$ follows the Boltzmann distribution law. Then, after interacting with a plane-wave clock laser at a Lamb-Dicke regime [26], the atoms follow a Rabi oscillation between the internal states with different Rabi frequencies according to their external states; and the bare Rabi frequency is $\Omega_0/2\pi \approx 9.0 \text{ Hz}$.

Longitude modulation.—The frequency of the lattice laser is modulated as $\omega_L(t) = \bar{\omega}_L + \omega_a \sin(\omega_s t + \psi)$ with $\bar{\omega}_L = 2\pi c/\lambda_L$, and ω_a is the driving amplitude [26,32]. In the lattice comoving frame, due to the relativistic Doppler effect, the atoms feel an effective clock frequency $\omega'_p(t) = \omega_p - A \cos(\omega_s t + \psi)$ with a driving amplitude $A = \omega_a \omega_p \omega_s L / c \bar{\omega}_L$ (L is the distance from the high-reflecting mirror to the lattice center). Then, the system can be approximately described with time-dependent Hamiltonian

$$\hat{H}_L = \hbar \left(\frac{\delta + A \cos(\omega_s t + \psi)}{2} \sigma_z + \frac{\Omega_{\vec{n}}}{2} \sigma_x \right). \quad (2)$$

As presented in our recent experiment [32], more than ten resolved Floquet sidebands are clearly observed. Both the theory and experiment indicate that the initial phase ψ is irrelevant to both the Rabi oscillation and spectrum.

Transverse modulation.—To modulate the Rabi frequency, we implement the amplitude modulation on the clock laser. Because the Rabi frequency is proportional to the square root of clock laser’s intensity $\Omega(t) \propto \sqrt{I(t)}$, we set the modulation function as $S_{PW}(t) = \cos^2(\omega_s t)$. However, the additional π phase is automatically inserted at the zero point $\Omega(t) = 0$, and it causes the discontinuity. To compensate for the phase, as demonstrated in Fig. 2(a), we utilize the phase modulation following the square wave oscillating between zero and ϕ [26]. Then, the Hamiltonian after rotating wave approximation (RWA) can be written as

$$\hat{H}_T = \frac{\hbar\delta}{2} \sigma_z + \frac{\hbar\Omega_{\vec{n}}}{2} \cos \omega_s t (\sigma_+ e^{if(t)} + \text{H.c.}), \quad (3)$$

with the effective phase modulation function $f(t)$ as

$$f(t) = \begin{cases} 0 & -T/4 \leq t - nT < T/4 \\ \pi - \phi & T/4 \leq t - nT < 3T/4 \end{cases}. \quad (4)$$

where $T = 2\pi/\omega_s$ is the modulation period. The Rabi frequency is under both amplitude and phase modulation as shown in Fig. 2(a). Because the experiment was run in the parameter region where the resolved sideband approximation of $\omega_s \gg \Omega_{\vec{n}}$ holds, the lowest order effective Hamiltonian derived from Floquet-Magnus expansion for n_t th Floquet sidebands is expressed as

$$\hat{H}_{Te}^{n_t} = \frac{\hbar\delta_{n_t}}{2}\sigma_z + \left(\frac{\hbar\Omega_{\vec{n}}^{n_t}}{2}\sigma_+ + \text{H.c.}\right), \quad (5)$$

in which $\delta_{n_t} = \delta - n_t\omega_s$, and the effective Rabi frequency is

$$\Omega_{\vec{n}}^{n_t} = \begin{cases} \frac{\Omega_{\vec{n}}(1-e^{-i\phi})}{4} & n_t = \pm 1 \\ -\frac{\Omega_{\vec{n}}(1+e^{i\phi})e^{(in_t\pi)/2}}{\pi(n_t^2-1)} & n_t = 2m \\ 0 & \text{others} \end{cases} \quad (6)$$

Then, the probability of internal excited states is

$$P_e^{n_t}(\delta, t) = \sum_{\vec{n}} q(\vec{n}) \left| \frac{\Omega_{\vec{n}}^{n_t}}{R_{\vec{n}}^{n_t}} \right|^2 \sin^2\left(\frac{R_{\vec{n}}^{n_t}}{2} t\right), \quad (7)$$

where $R_{\vec{n}}^{n_t} = \sqrt{|\Omega_{\vec{n}}^{n_t}|^2 + \delta_{n_t}^2}$ with the Boltzmann distribution factor $q(\vec{n})$ of external states $|\vec{n}\rangle$ [25]. In Fig. 2(b), the experimental Rabi spectrum at a measuring time of $t = 70$ ms matches well with the theoretical result. To remove the phase discontinuity of amplitude modulation, we set $\phi = \pi$ for total compensation. As demonstrated in Fig. 2(c), all the Floquet channels are totally suppressed

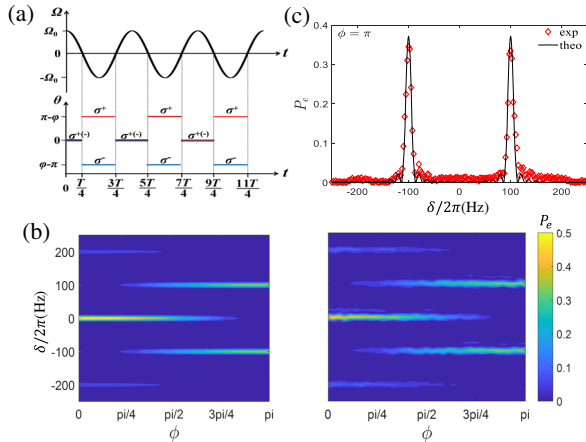


FIG. 2. Transverse modulation. (a) Rabi frequency simultaneously under a sinusoidal waveform amplitude modulation and a square waveform phase modulation. (b) Rabi spectrum of theoretical prediction (left) and experimental results (right) for phase ϕ changing from zero to π at measuring time $t = 70$ ms. (c) Comparison between experimental and theoretical Rabi spectra with $\phi = \pi$.

down to weaker than noise, except for $n_t = \pm 1$ Floquet channels with equal height [26].

Double modulation and interference.—Longitude and transverse modulations are demonstrated to be well fine-tuned, respectively. However, the modulation of one parameter should not affect another one for double modulation. Meanwhile, both modulations must be synchronized to make their relative phase ψ finely tunable and stable [26]. To achieve that, we use a function generator to generate both modulation functions with the same frequency and chose it as low as $\omega_s/2\pi = 100$ Hz. After the RWA, the system can be well described with the explicit form of Eq. (1):

$$\hat{H}_D = \hbar \left[\frac{\delta + A \cos(\omega_s t + \psi)}{2} \sigma_z + \frac{\Omega_{\vec{n}}}{2} \cos(\omega_s t) \sigma_x \right]. \quad (8)$$

Then, if we consider both modulations can produce a set of Floquet quasienergy spectra with the same intervals, a question will immediately arise—Could the relative phase make different Floquet channels interfere so that the Rabi spectra changed?

In our experiment, we only vary the relative phase without changing other parameters. As shown in Figs. 3(a)–3(c), the Rabi spectra strongly change according to ψ . There are two main features that can be clearly observed: (I) the different Floquet sidebands undergo different destructive or constructive interference processes; and (II) the spectrum at ψ and $\pi - \psi$ are the same, which reflects a hidden symmetry. In order to reveal its mechanism, utilizing the Jacobi-Anger relation and Floquet theory, we obtain the effective Floquet Hamiltonian similar to Eq. (5) but with a different effective Rabi frequency for the n_d th Floquet sideband:

$$\Omega_{\vec{n}}^{n_d} = \frac{e^{in_d\psi}\Omega_{\vec{n}}}{2} (J_{n_d-1}[K]e^{-i\psi} + J_{n_d+1}[K]e^{i\psi}), \quad (9)$$

in which $K = A/\omega_s$ is the renormalized driving amplitude, and where $J_n[\]$ is the n th order first kind Bessel function [26]. Together with Eq. (7), we could calculate the Rabi spectrum; and Figs. 3(a)–3(c) demonstrate that the theoretical results are quite consistent with the experimental data.

The interference can be understood via expression of the effective Rabi frequency [Eq. (9)]. The n_d th Floquet frequency has two terms that are related to $n_d \pm 1$ Floquet modes of longitude modulation, respectively. As demonstrated in Figs. 1(b) and 1(c), in the dressed atom picture, the longitude modulation provides lots of Floquet photons carrying the ψ phase. Meanwhile, if the transverse modulation is also on, the hopping from $|g\rangle$ to $|e\rangle$ states can have two channels: ω_p^+ and ω_p^- . Because both modulations have the same driving frequency of $\omega_s^x = \omega_s^z = \omega_s$, when $\omega_p^+ + (n_d - 1)\omega_s = \omega_p^- + (n_d + 1)\omega_s$ is equal to the gap Δ , the

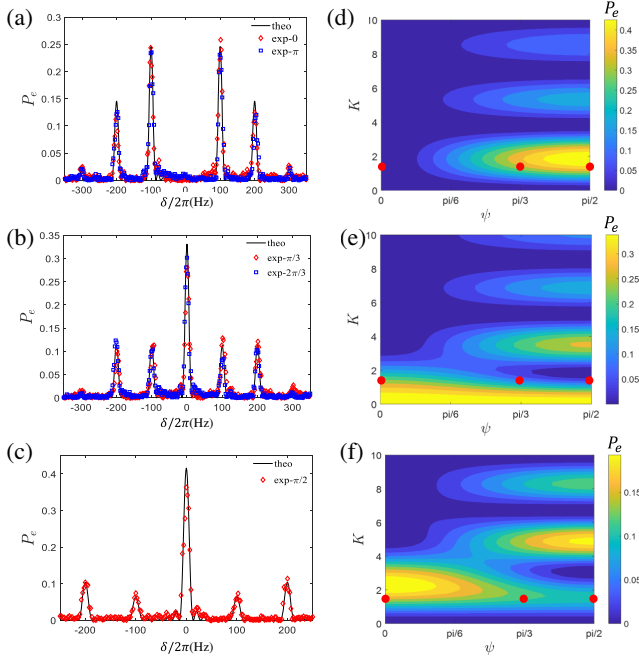


FIG. 3. Rabi spectrum of double modulation. (a)–(c) Comparisons between theoretical and experimental results for different ψ at $K = 1.38$. (d)–(f) Peak’s height of zeroth to second order Floquet sidebands at measuring time of $t = 70$ ms calculated with Floquet theory, where red dots mark parameters chosen in Figs. 3(a)–3(c).

atoms can be excited via both channels. Considering the phase difference between both channels is 2ψ , the atoms can interfere with each other, and the period is π . From the theoretically calculated heights of zeroth to second order Floquet sideband peaks shown in Figs. 3(d)–3(f), we can find that the interference of all Floquet sidebands could be observed by adjusting the renormalized driving amplitude K . Then, because the Bessel functions are real, the strongest interference effect happens at ψ equal to zero and $\pi/2$. In addition, because the probability of excitation P_e is irrelevant to the argument of the Rabi frequency, the Rabi spectra at ψ and $\pi - \psi$ are the same. Furthermore, for a different driving frequency, the Floquet spectrum will be nearly unchanged via rescaling detuning with the unit of the driving frequency (see Supplemental Material [26] for different ω_s at $K = 1.1$).

Double modulation and topology.—The n_d th sideband effective Floquet Hamiltonian of the doubly modulated OLC could also be taken as a spin 1/2 atom coupled to two magnetic fields of $H_{\text{EF}}^{n_d} = (\hbar/2)(\vec{h}_{n_d} \times \vec{\sigma})$ with $\vec{h}_{n_d} = \vec{B}_{n_d-1} + \vec{B}_{n_d+1}$ and

$$\vec{B}_{n_d} = \frac{\Omega_{\vec{n}} J_{n_d}[K]}{2} \left\{ \cos(n_d \psi), -\sin(n_d \psi), \frac{\delta - n_d \omega_s}{\Omega_{\vec{n}} J_{n_d}[K]} \right\}.$$

Then, we can consider $h_{n_d}^z = 0$, where the peak of the n_d th order Floquet sideband stands. Reminiscent of the famous Su-Schrieffer-Heeger (SSH) model in momentum space of $H_{\text{SSH}} = \vec{h}(k) \times \vec{\sigma}$ [34,35], the numbers of effective Hamiltonians $H_{\text{EF}}^{n_d}$ can be provided for simulating various 1D quantum topological phases after mapping the phase ψ to quasimomentum k . Similar to analyzing the endpoint of $\vec{h}(k)$ while letting the quasimomentum k walk around the Brillouin zone, we can also check different $\vec{h}_{n_d}(\psi)$ while varying ψ from $-\pi$ to π . Meanwhile, the eigenenergies $E_{n_d}^{\pm}(\psi) = \pm(\hbar|\vec{h}_{n_d}|)/2$ can also be calculated for checking the close of the energy gap. Because the Rabi oscillation is only related to the modulus of the effective Rabi frequency $|\vec{h}_{n_d}|$, we can experimentally measure the Rabi oscillation and extract the eigenenergies of different Floquet sidebands [26].

For the zeroth Floquet sideband, the effective total magnetic field is $\vec{h}_0 = \{0, -2J_1[K] \sin(\psi), 0\}$ since $J_{-1}[K] = -J_1[K]$. Then, because \vec{h}_0 only has a nonzero y component, the system cannot have nontrivial topology. Turning to the first order Floquet sideband, in Fig. 4(a), the experimental result of eigenenergies shows the energy gap closed at

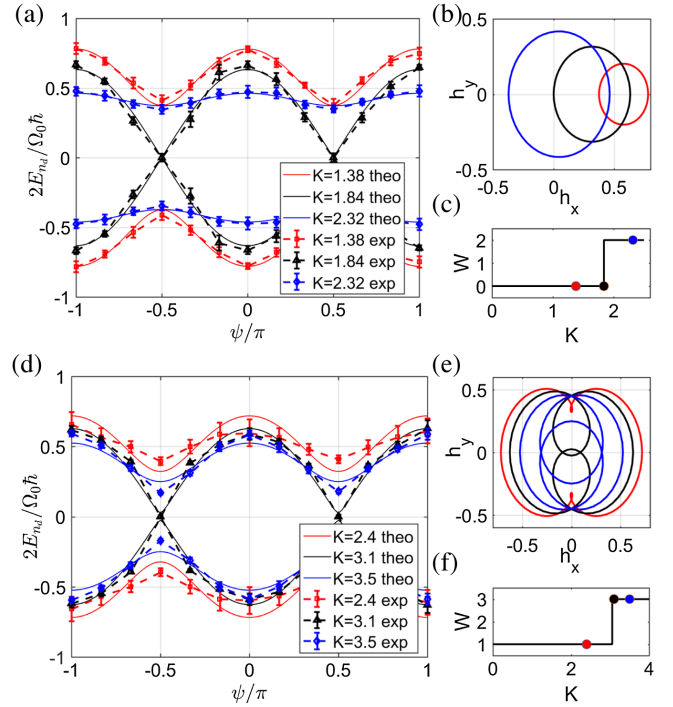


FIG. 4. Topology of Floquet effective Hamiltonians. (a) Eigenenergies in units of bare Rabi frequency Ω_0 of the first order Floquet sideband for different K obtained theoretically (solid line) and experimentally (dashed line). Corresponding theoretical results of “magnetic field” in $h_x - h_y$ plane and winding number shown in Figs. 4(b) and 4(c) corresponding to same color in Fig. 4(a). Results of second order Floquet sideband shown in Figs. 4(d)–4(f).

$K = 1.84$. From the Rabi spectrum around it [26], we obtain the experimental value with uncertainty of $K_{c1}^E = 1.84(8)$, which agrees well with the theoretical prediction $K_{c1}^T = 1.8412$. When tuning the phase ψ from $-\pi$ to π , the effective magnetic field can form a closed path. In Fig. 4(b), we can find that the origin point moves from outside to inside by increasing K , and the touch point corresponds to the parameter at which the energies have the linear dispersion around the gap's closed point of $\psi = \pm\pi/2$. The small deviations between theoretical and experimental results at the low effective Rabi frequency are due to the dephasing of the Rabi oscillation [33,36]. In order to quantitatively analyze the topology, we have to calculate the winding number

$$W = \frac{1}{2\pi i} \int_{-\pi}^{\pi} \frac{d \ln(h_{n_d}^x - ih_{n_d}^y)}{d\psi} d\psi,$$

which is a topological invariant. As shown in Fig. 4(c), winding numbers equal to zero and two correspond to the origin points outside and inside the closed path, respectively. The linear dispersion is related to the topological transition point from zero to two, as well as the closed path touching from the negative h_x direction. The topological transition of the second order Floquet sideband is shown in Figs. 4(d)–4(f), and the winding number changes from one to three. The topological transition point $K_{c2}^E = 3.10(11)$ [26] is also related to the linear dispersion of energy at $\psi = \pm\pi/2$. Differently, the closed path touches the origin point from both $\pm h_y$ directions.

These topological properties can be theoretically understood by analyzing two effective magnetic fields \vec{B}_{n_d-1} and \vec{B}_{n_d+1} , of which the winding numbers are $n_d - 1$ and $n_d + 1$, respectively. Because the total magnetic field \vec{h}_{n_d} is homotopic to one effective magnetic field, which has a larger magnitude, the winding number of the system is determined by B_n with larger magnitude. When the renormalized driving amplitude K is small, the magnitude of \vec{B}_{n_d-1} is larger than \vec{B}_{n_d+1} , and so the winding number is $n_d - 1$. Then, when $|\vec{B}_{n_d-1}|$ is equal to $|\vec{B}_{n_d+1}|$, we obtain the first critical point where the winding number changes from $n_d - 1$ to $n_d + 1$. Considering the $|\vec{B}_{n_d-1}| - |\vec{B}_{n_d+1}|$ alternative changing around zero, the winding number should oscillate between $n_d - 1$ and $n_d + 1$.

Conclusion and outlook.—We successfully realized double modulation in the OLC platform. By fine-tuning the relative phase between both modulations, we observed the clear interference effect induced by two types of Floquet photons. Meanwhile, we find they are strongly related to the 1D topological insulator and experimentally observed the energy gap open-close-open behavior. Beyond the SSH model, the high order effective Floquet Hamiltonians preserve higher winding numbers.

In the OLC platform, the coherence time could last at least more than 6 s [37], and so the topological phase transition and the related physics of dynamics can be finely studied in the future work. In addition, the realization of double modulation can open several research paths. The straightforward way is extending the simulation of the topological insulator from 1D to two dimensions by tuning the compensated phase ϕ . Meanwhile, a more complex topological phase can be simulated by combining with other degrees of freedom [38]. On the other hand, choosing two driving frequencies incommensurately or opening the tunneling of nearest neighbor lattice sites [24] may also bring in chaos or exotic many-body Hamiltonians.

X.-F.Z. is thankful for valuable discussions with Z.-J. Xiong and S.-X. Qin. This work is supported by the National Science Foundation of China (Grant No. 61775220), the Key Research Project of Frontier Science of the Chinese Academy of Sciences (Grant No. QYZDB-SSW-JSC004), and the Strategic Priority Research Program of the Chinese Academy of Sciences (Grants No. XDB21030100 and No. XDB35010202). T.W. is supported by the Special Foundation for Theoretical Physics Research Program of China (Grant No. 11647165) and the China Postdoctoral Science Foundation Funded Project (Project No. 2020M673118). X.-F.Z. acknowledges funding from the National Science Foundation of China under Grants No. 11804034, No. 11874094, and No. 12047564, as well as from Fundamental Research Funds for the Central Universities under Grant No. 2020CDJQY-Z003.

*zhangxf@cqu.edu.cn

†changhong@ntsc.ac.cn

‡These authors contributed equally to this work.

- [1] A. Eckardt, *Rev. Mod. Phys.* **89**, 011004 (2017).
- [2] T. Oka and S. Kitamura, *Annu. Rev. Condens. Matter Phys.* **10**, 387 (2019).
- [3] P. Kiefer, F. Hakeberg, M. Wittemer, A. Bermúdez, D. Porras, U. Warring, and T. Schaetz, *Phys. Rev. Lett.* **123**, 213605 (2019).
- [4] P. Roushan *et al.*, *Nat. Phys.* **13**, 146 (2017).
- [5] Z. Shu, Y. Liu, Q. Cao, P. Yang, S. Zhang, M. B. Plenio, F. Jelezko, and J. Cai, *Phys. Rev. Lett.* **121**, 210501 (2018).
- [6] S. Mukherjee, M. Di Liberto, P. Öhberg, R. R. Thomson, and N. Goldman, *Phys. Rev. Lett.* **121**, 075502 (2018).
- [7] F. Mei, Q. Guo, Y.-F. Yu, L. Xiao, S.-L. Zhu, and S. Jia, *Phys. Rev. Lett.* **125**, 160503 (2020).
- [8] X. G. Wen, F. Wilczek, and A. Zee, *Phys. Rev. B* **39**, 11413 (1989).
- [9] F. Görg, K. Sandholzer, J. Minguzzi, R. Desbuquois, M. Messer, and T. Esslinger, *Nat. Phys.* **15**, 1161 (2019).
- [10] S. Greschner, L. Santos, and D. Poletti, *Phys. Rev. Lett.* **113**, 183002 (2014).
- [11] H. Zhao, J. Knolle, and F. Mintert, *Phys. Rev. A* **100**, 053610 (2019).

- [12] H. Zhao, J. Vovrosh, F. Mintert, and J. Knolle, *Phys. Rev. Lett.* **124**, 160604 (2020).
- [13] Y. Zheng and S. Yang, *New J. Phys.* **18**, 013005 (2016).
- [14] M. Takamoto, F.-L. Hong, R. Higashi, and H. Katori, *Nature (London)* **435**, 321 (2005).
- [15] A. D. Ludlow, M. M. Boyd, J. Ye, E. Peik, and P. O. Schmidt, *Rev. Mod. Phys.* **87**, 637 (2015).
- [16] N. Poli, C. W. Oates, P. Gill, and G. M. Tino, *Riv. Nuovo Cimento Soc. Ital. Fis.* **36**, 555 (2013).
- [17] H. Katori, M. Takamoto, V. G. Palchikov, and V. D. Ovsiannikov, *Phys. Rev. Lett.* **91**, 173005 (2003).
- [18] P. G. Westergaard, J. Lodewyck, L. Lorini, A. Lecallier, E. A. Burt, M. Zawada, J. Millo, and P. Lemonde, *Phys. Rev. Lett.* **106**, 210801 (2011).
- [19] G. E. Marti, R. B. Hutson, A. Goban, S. L. Campbell, N. Poli, and J. Ye, *Phys. Rev. Lett.* **120**, 103201 (2018).
- [20] L. Sonderhouse, C. Sanner, R. B. Hutson, A. Goban, T. Bilitewski, L. Yan, W. R. Milner, A. M. Rey, and J. Ye, *Nat. Phys.* **16**, 1216 (2020).
- [21] M. S. Safronova, D. Budker, D. DeMille, D. F. Jackson Kimball, A. Derevianko, and C. W. Clark, *Rev. Mod. Phys.* **90**, 025008 (2018).
- [22] S. Kolkowitz, I. Pikovski, N. Langellier, M. D. Lukin, R. L. Walsworth, and J. Ye, *Phys. Rev. D* **94**, 124043 (2016).
- [23] M. A. Norcia, J. R. K. Cline, and J. K. Thompson, *Phys. Rev. A* **96**, 042118 (2017).
- [24] S. Kolkowitz, L. Bromley, T. Bothwell, M. L. Wall, G. E. Marti, A. P. Koller, X. Zhang, A. M. Rey, and J. Ye, *Nature (London)* **542**, 66 (2017).
- [25] S. Blatt, J. W. Thomsen, G. K. Campbell, A. D. Ludlow, M. D. Swallows, M. J. Martin, M. M. Boyd, and J. Ye, *Phys. Rev. A* **80**, 052703 (2009).
- [26] See Supplemental Material at <http://link.aps.org/supplemental/10.1103/PhysRevLett.127.033601> for more details about the experimental realizations, Floquet methods, driving stability, frequency shift, eigenenergy measurement, and uncertainty of K_c , which includes Refs. [25,27–33].
- [27] H. Lignier, C. Sias, D. Ciampini, Y. Singh, A. Zenesini, O. Morsch, and E. Arimondo, *Phys. Rev. Lett.* **99**, 220403 (2007).
- [28] G. K. Campbell *et al.*, *Science* **324**, 360 (2009).
- [29] A. Goban, R. B. Hutson, G. E. Marti, S. L. Campbell, M. A. Perlin, P. S. Julienne, J. P. D’Incao, A. M. Rey, and J. Ye, *Nature (London)* **563**, 369 (2018).
- [30] M. D. Swallows *et al.*, *IEEE Trans. Ultrason. Ferroelectr. Freq. Control* **59**, 416 (2012).
- [31] M. J. Martin, M. Bishof, M. D. Swallows, X. Zhang, C. Benko, J. von Stecher, A. V. Gorshkov, A. M. Rey, and J. Ye, *Science* **341**, 632 (2013).
- [32] M.-J. Yin, T. Wang, X.-T. Lu *et al.*, *Chin. Phys. Lett.* **38**, 073201 (2021).
- [33] A. M. Rey, A. V. Gorshkov, C. V. Kraus, M. J. Martin, M. Bishof, M. D. Swallows, X. Zhang, C. Benko, J. Ye, N. D. Lemke, and A. D. Ludlow, *Ann. Phys. (Amsterdam)* **340**, 311 (2014).
- [34] A. J. Heeger, S. Kivelson, J. R. Schrieffer, and W. P. Su, *Rev. Mod. Phys.* **60**, 781 (1988).
- [35] M. Z. Hasan and C. L. Kane, *Rev. Mod. Phys.* **82**, 3045 (2010).
- [36] L. Marmet and A. A. Madej, *Can. J. Phys.* **78**, 495 (2000).
- [37] S. L. Campbell *et al.*, *Science* **358**, 90 (2017).
- [38] R. Zhang, Y. Cheng, P. Zhang, and H. Zhai, *Nat. Rev. Phys.* **2**, 213 (2020).